

# Hydrogen Bond Migration between Molecular Sites Observed with Ultrafast 2D IR Chemical Exchange Spectroscopy

Daniel E. Rosenfeld, Kyungwon Kwak, Zsolt Gengeliczki, and M. D. Fayer\*

Department of Chemistry, Stanford University, Stanford, California 94305

Received: December 2, 2009; Revised Manuscript Received: January 12, 2010

Hydrogen-bonded complexes between phenol and phenylacetylene are studied using ultrafast two-dimensional infrared (2D IR) chemical exchange spectroscopy. Phenylacetylene has two possible  $\pi$  hydrogen bonding acceptor sites (phenyl or acetylene) that compete for hydrogen bond donors in solution at room temperature. The OD stretch frequency of deuterated phenol is sensitive to which acceptor site it is bound. The appearance of off-diagonal peaks between the two vibrational frequencies in the 2D IR spectrum reports on the exchange process between the two competitive hydrogen-bonding sites of phenol–phenylacetylene complexes in the neat phenylacetylene solvent. The chemical exchange process occurs in  $\sim 5$  ps and is assigned to direct hydrogen bond migration along the phenylacetylene molecule. Other nonmigration mechanisms are ruled out by performing 2D IR experiments on phenol dissolved in the phenylacetylene/carbon tetrachloride mixed solvent. The observation of direct hydrogen bond migration can have implications for macromolecular systems.

## I. Introduction

Weak intermolecular  $\pi$ -hydrogen-bonding interactions are important determinants of the specificity of intermolecular recognition processes and of self-assembly processes in both synthetic and biological systems.<sup>1,2</sup> When acting in concert, these interactions provide global structural stability. An important design criterion for self-assembling systems is the trade-off between thermodynamic stability and kinetic freedom.<sup>3</sup> Understanding the detailed kinetic mechanisms that can connect supramolecular states and their associated time scales facilitates design of stable and rapidly forming supramolecular complexes. Generating such a kinetic model for the individual weak interactions in supramolecular complexes is difficult due to the intrinsic experimental challenges of ultrafast kinetics measurements under thermal equilibrium conditions. In this article, we examine the motion of an electrophile along a conjugated  $\pi$  system. We show that, for such a system, direct migration of the electrophile along the conjugated molecule is possible and is the dominant mechanism for exchange between different  $\pi$ -base sites on a conjugated backbone.

The specific system we investigate is the hydrogen-bonding complex formed between deuterated phenol and phenylacetylene. When phenol is dissolved in an aromatic  $\pi$ -base solvent, weak hydrogen-bonding complexes form.<sup>4</sup> These complexes can be observed with infrared absorption spectroscopy, as the hydrogen-bonding interaction shifts the absorption of the OD stretch to lower frequency (red shifts).<sup>4–8</sup> Phenylacetylene consists of a benzene ring with a single bond to one of the two triply bonded carbons of acetylene. This molecule possesses two independent hydrogen-bonding sites (the benzene ring and the triple bond) that have different hydrogen-bonding energies when bound to hydrogen bond donors, notably phenol.<sup>7</sup> These hydrogen-bonding sites are in a competitive equilibrium at room temperature.<sup>7,9</sup>

Phenol and phenylacetylene have previously been investigated by infrared absorption spectroscopy in solution.<sup>7</sup> The study

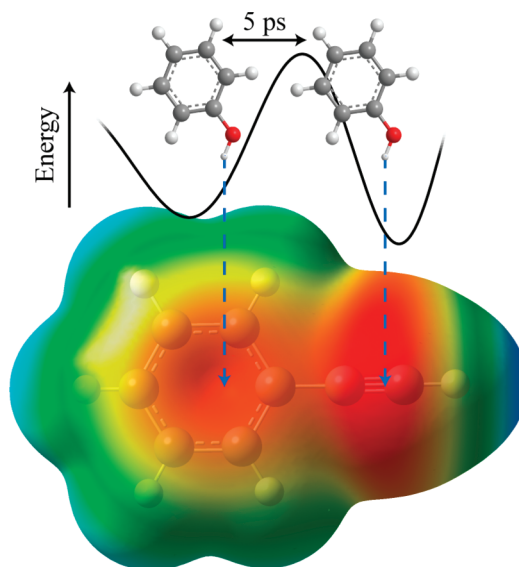


**Figure 1.** A molecular electrostatic potential energy map of the phenylacetylene molecule (calculated with DFT at the B3LYP/6-311G(d,p) level of theory). Blue corresponds to electrostatic potentials  $\geq 20$  kcal/mol, and red corresponds to electrostatic potentials  $\leq -14$  kcal/mol. The limits have been adjusted for high contrast. Superimposed is a schematic of phenol hydrogen bond migration along the phenylacetylene. The black curve is a qualitative rendering of the expected electrostatic interaction.

showed that the two hydrogen-bonding sites shift the frequency of the OD stretch by different amounts. Other hydrogen bond donors (HF, H<sub>2</sub>O, NH<sub>3</sub>) have been investigated with phenylacetylene in gas-phase spectroscopic studies and theoretically.<sup>9–14</sup> These studies elucidate the structures of hydrogen-bonding complexes with phenylacetylene in the gas phase and confirm the presence of two hydrogen-bonding sites. To graphically illustrate the hydrogen-bond-accepting sites of phenylacetylene, Figure 1 depicts the molecular electrostatic potential map of phenylacetylene. Red indicates negative charge density, and clearly the triple bond is more negatively charged than the ring.

\* To whom correspondence should be addressed. E-mail: fayer@stanford.edu.

Therefore, the triple bond has a stronger electrostatic affinity, which is a significant component of the hydrogen bond formation driving force in these systems.<sup>15,16</sup> Also shown in the figure is a cartoon for hydrogen bond migration. We will demonstrate that direct migration is the primary exchange mechanism that mediates the competitive equilibrium between these sites. By direct migration we mean that the hydrogen bond switches between sites on the same molecule without dissociating from one site and rebinding to the other site on a different molecule. In effect, the hydrogen bond slides back and forth between binding sites on a single phenylacetylene molecule.

Phenylacetylene can be polymerized to form poly(phenylacetylene), a highly conjugated polymer which forms folded structures in solution.<sup>17</sup> This polymer has been used as model system for investigating polymer folding.<sup>17</sup> The primary folding mechanism is solvophobicity. However, there are significant interatomic interactions that can contribute to the stability of three-dimensional structures of the polymer.<sup>17</sup> Functionalized poly(phenylacetylene) and analogues have been of great interest due to the ease of control over their chiral, optical, and structural properties.<sup>18–21</sup> An important interaction within such aromatic systems is the face-to-edge  $\pi$ – $\pi$  coupling that leads to the formation of T-shaped complexes.<sup>15,16,22</sup> This interaction is also important in crystal formation.<sup>23</sup> This type of coupling is substantially electrostatic and occurs between the positively polarized  $\sigma$ -bond network of one aromatic molecule and the negative  $\pi$  cloud of another.<sup>15,16</sup> The hydrogen bond formed between phenol and a  $\pi$  system also has a large electrostatic component.<sup>15,16,22</sup> The dynamics of the system studied here can provide insight into the more common face-to-edge  $\pi$ – $\pi$  interaction in conjugated systems as the two types of interaction have similar origins and magnitude. Furthermore, if we can understand how the phenol moves between sites on phenylacetylene, it is reasonable to conclude that similar motions are possible for any electrostatically interacting site that encounters the partially charged surface of a conjugated system.

The primary goal of this study is to investigate the dynamics of the phenol/phenylacetylene system and to determine the underlying kinetics and mechanism of the competitive equilibrium which occurs between the two hydrogen-bonding sites on phenylacetylene. The tool employed for the kinetic study is ultrafast two-dimensional infrared (2D IR) chemical exchange spectroscopy. The technique is akin to 2D NMR chemical exchange techniques that typically operate on a millisecond time scale. The 2D IR method can measure chemical exchange using vibrational resonances on the femtosecond and picosecond time scales. This nonlinear spectroscopic method has been used in the past to investigate the thermal equilibrium dynamics of  $\pi$ -hydrogen-bonding complexes,<sup>24–26</sup> rotational isomerization,<sup>27</sup> protein substate switching,<sup>28</sup> the exchange of chloroform between complexes with acetone and DMSO in an acetone/DMSO mixed solvent,<sup>29</sup> and water hydrogen bond exchange between an ion and another water molecule.<sup>30,31</sup>

Of particular importance for the work presented here are the previous studies of the thermal equilibrium dissociation–formation kinetics of weakly bound  $\pi$ -hydrogen-bonding complexes between phenol and aromatic compounds.<sup>5,6,25,32</sup> For example, hydrogen bond formation and dissociation of the phenol  $\pi$ -hydrogen bonding with benzene in a mixed solvent of benzene and carbon tetrachloride were studied with chemical exchange spectroscopy.<sup>33</sup> Phenol is either bound to benzene or it is dissociated and unbound, which is referred to as free phenol. Free phenol and phenol bound to benzene have distinct hydroxyl stretch frequencies as seen in an FT-IR spectrum. In the 2D IR

chemical exchange experiment, at short time, there are two peaks on the diagonal of the 2D spectrum. Dissociation and formation of complexes causes off-diagonal peaks to grow in. The time-dependent growth of the off-diagonal peaks is directly related to the rates of complex formation and dissociation under thermal equilibrium conditions. Thirteen  $\pi$ -hydrogen-bonding complexes have been studied with chemical exchange spectroscopy.<sup>5</sup> For each complex, the formation/dissociation rate has been determined, and it was shown that the rates are directly related to the enthalpy of formation of the complex.

In this study, the 2D IR chemical exchange technique is used to measure the phenol  $\pi$  hydrogen bond exchange time between the ring and triple bond acceptor sites of phenylacetylene. The measurement of the exchange time between the two hydrogen-bonding states cannot fully determine the mechanism for the process. Several alternative mechanistic hypotheses are viable for such a system. The hypothesis that we will show to be correct is that the phenol molecule migrates along the phenylacetylene back and forth between the ring and the triple bond accepting site. However, exchange between these two hydrogen-bonding states might also occur via intermolecular hopping within a single solvation shell or via an intermediate free state that is not hydrogen bonded. To address the alternative mechanisms for the phenol/phenylacetylene system, we dilute the phenol/phenylacetylene mixture with carbon tetrachloride. The diluted sample permits direct observation of the free non-hydrogen-bonded state. Furthermore, by diluting the sample, discrimination between the intermolecular hopping and intramolecular migration mechanisms is achieved as the mechanisms depend differently on the concentration of phenylacetylene in solution.

## II. Experimental Methods

The 2D IR vibrational echo experimental method has been previously described in depth; however, a brief description will be included here.<sup>25,32,34,35</sup> Three ultrashort mid-infrared laser pulses with duration of 70 fs, bandwidth 250  $\text{cm}^{-1}$ , energy 500 nJ, and center frequency 2650  $\text{cm}^{-1}$ , are generated by optical parametric amplification and subsequent difference frequency mixing of the output of a regeneratively amplified Ti:sapphire laser system (40 fs, 600  $\mu\text{J}$ , 800 nm). These three pulses are focused into a liquid sample in a BOXCAR geometry.

In the three-pulse sequence, the time between pulses 1 and 2 is called  $\tau$ , and the time between pulses 2 and 3 is called  $T_w$ . A fourth pulse, the vibrational echo, which is the signal in the experiment, is emitted at a time  $\leq \tau$  after the third pulse. The vibrational echo pulse is combined with another pulse, the local oscillator, for heterodyne detection. During the first time period,  $\tau$ , the vibrational oscillators exist in coherent superpositions of the ground and first excited vibrational states and their phases evolve at frequencies  $\omega_\tau$  ( $\omega_\tau$  is the horizontal axis of the 2D spectra). The second laser pulse (the start of the  $T_w$  period) ends the coherence period and places the vibrational oscillators into either a population of the first vibrational excited state or the ground vibrational state. Following the third pulse, the oscillators are again in superposition states, and the vibrational echo is emitted. The third pulse produces superposition states of both the 0–1 and 1–2 to transitions, resulting in vibrational echo emission at the 0–1 transition frequency and at the 1–2 transition frequency, which is shifted to lower frequency by the vibrational anharmonicity. The combined vibrational echo pulse and the local oscillator are passed through a monochromator acting as a spectrograph and detected with an MCT array. Taking the spectrum performs one of the two Fourier transforms necessary to obtain the 2D spectrum, providing the vertical  $\omega_m$

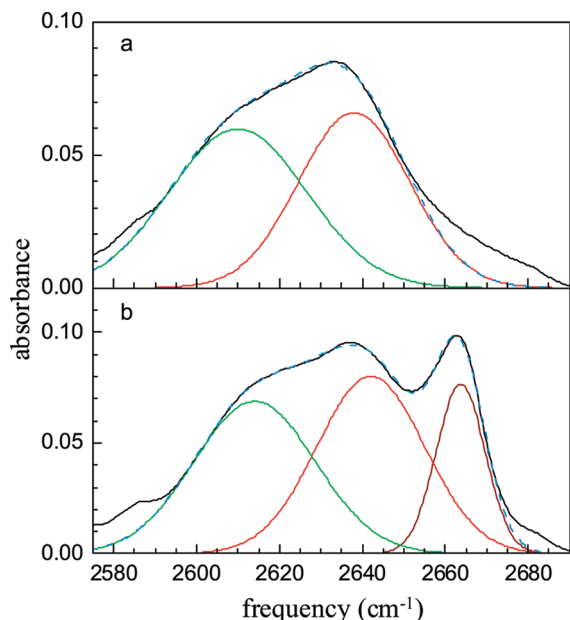


**Figure 2.** Linear absorbance spectra for phenol in pure phenylacetylene (a) and phenol dissolved in a phenylacetylene and carbon tetrachloride mixture (b) (black curves). Also shown are fits to two and three Gaussians in a and b, respectively (blue dashed curves). The Gaussians that comprise the fits are also shown. The unfit portions of the spectral wings are most likely due to changes in the strong phenylacetylene background upon complexation that cannot be subtracted and also the light tails of the Gaussian line-shape function. Also, other subensembles of complexes may be present in small amounts. Our models were only fit over the strongly peaked portions of the spectra.

axis. Each pixel in the array measures an interferogram as  $\tau$  is scanned. Numerical Fourier transforms of the interferograms produce the spectrum along the  $\omega_\tau$  axis. For a given fixed  $T_w$ ,  $\tau$  is scanned to produce a single 2D spectrum. Then  $T_w$  is changed, and  $\tau$  is again scanned to produce another 2D spectrum. The time evolution of the 2D spectra vs  $T_w$  provides the dynamical information for the system. When the sample consists of two chemically exchanging subensembles with different vibrational frequencies, the time dependence of the growth of the off-diagonal peaks reports on the equilibrium chemical exchange kinetics.

Deuterated phenol was prepared by methods outlined previously.<sup>36</sup> All other chemicals were used as obtained from Sigma-Aldrich. Both linear absorbance and 2D IR measurements were made in a 250  $\mu\text{m}$  sample cell with  $\text{CaF}_2$  windows; the concentration of deuterated phenol used was always about 0.1 M.

### III. Results and Discussion

**A. Linear and 2D IR Spectroscopic Data.** The infrared absorbance spectrum of deuterated phenol dissolved in pure phenylacetylene is shown in Figure 2a. The spectrum (black curve) has two highly overlapping absorbance bands that are centered at 2638 and 2610  $\text{cm}^{-1}$ . Gaussian fits of the two absorption bands (green and red curves) and their sum (dashed blue curve) are also shown. From the fits, the full width at half-maxima (fwhm) of the absorbances are 31.6 and 39  $\text{cm}^{-1}$ , respectively. Previous theory and gas-phase experiments on other hydrogen-bonded complexes with phenylacetylene have shown that a larger vibrational shift to lower frequency occurs when the hydrogen bond donor is locally associated with the triple bond.<sup>10–12,14,37</sup> We therefore refer to the 2610  $\text{cm}^{-1}$  as the triple bond (T) state and the 2638  $\text{cm}^{-1}$  peak as the ring (R)

state. Such an assignment is also corroborated by examining the molecular electrostatic potential map displayed in Figure 1. A hydrogen bond formed with the triple bond is expected to be stronger than one formed with the ring state based on electrostatics. A variety of studies have found a correlation between hydrogen bond strength and the vibrational frequency shift, which would suggest that the OD stretch has a lower vibrational frequency when in the T hydrogen-bonding state.<sup>4,5</sup>

Figure 2b is the infrared absorbance spectrum of phenol and phenylacetylene dissolved in carbon tetrachloride (black curve). The mole ratio between phenylacetylene and carbon tetrachloride is 0.60. This mole ratio results in a reduction of the concentration (mol/L) of phenylacetylene by a factor of 2.5. Clearly evident is the non-hydrogen-bonded OD absorbance (free phenol) at 2664  $\text{cm}^{-1}$ . Three Gaussians are used to fit the spectrum (green, red, and wine curves); their sum is the dashed blue curve. The R and T hydrogen-bonding states have shifted to 2642 and 2614  $\text{cm}^{-1}$  and have Gaussian fwhm of 30.6 and 34.4  $\text{cm}^{-1}$ , respectively. These shifts reflect the changes in the solvation structure of the complexes when  $\text{CCl}_4$  is added to the solution. The free phenol OD absorption has a Gaussian fwhm of 13.8  $\text{cm}^{-1}$ . The inhomogeneous broadening of solute–solvent complexes by solvent shell variations have been discussed in detail previously.<sup>33</sup>

In Figure 3, the top row of panels shows three representative 2D IR spectra for deuterated phenol dissolved in pure phenylacetylene. These 2D IR spectra show the 0–1 (positive going) part of the each spectrum. The 1–2 (negative going) portions were measured but are not shown. At  $T_w = 200$  fs, there has been insufficient time for significant chemical exchange to occur. There are two peaks on the diagonal, corresponding to the two overlapping peaks in Figure 2. Inhomogeneous broadening causes the 2D bands to be elongated along the diagonal. However, both 2D bands have large homogeneous components that comprise substantial portions of the dynamic line shapes.<sup>33</sup> As the OD vibrational oscillators sample all frequencies within their respective absorption lines, the peaks become more round; this process is called spectral diffusion.<sup>35</sup> By  $T_w = 3$  ps the diagonal peaks appear quite round indicating that much of the dynamic broadening has occurred by this time. Because of the large homogeneous contributions, spectral diffusion is not the dominant factor contributing to the dynamic line shapes. In the  $T_w = 3$  ps spectrum, off-diagonal peaks between the two hydrogen bonding states are visible, and by  $T_w = 7$  ps these peaks are of a significant intensity relative to the main diagonal peaks. Because the frequency separation of the diagonal peaks is small, the off-diagonal chemical exchange peaks do not appear as distinct peaks. Rather, they overlap with the diagonal peaks and produce the almost square shape seen at  $T_w = 7$  ps. This shape has been observed previously in some 2D IR chemical exchange spectra.<sup>5</sup> The time dependence of the growth of the off-diagonal peaks reports on the kinetics of the exchange process between the R and T hydrogen-bonding states.

**B. Fitting the 2D IR Data.** The theoretical framework for analyzing kinetic processes measured by 2D IR chemical exchange spectroscopy has been reported previously.<sup>5,6,25,26</sup> A kinetic model is used in which each vibrational state undergoes chemical exchange, vibrational relaxation, and rotational diffusion. These processes are treated through an analytical solution to the corresponding differential equations.<sup>26</sup> The solution to the coupled differential equations is the sum of two contributions, one that is isotropic, i.e., it does not depend on the rotational diffusion constant, and one that does depend on rotational diffusion constants. These two terms are generaliza-

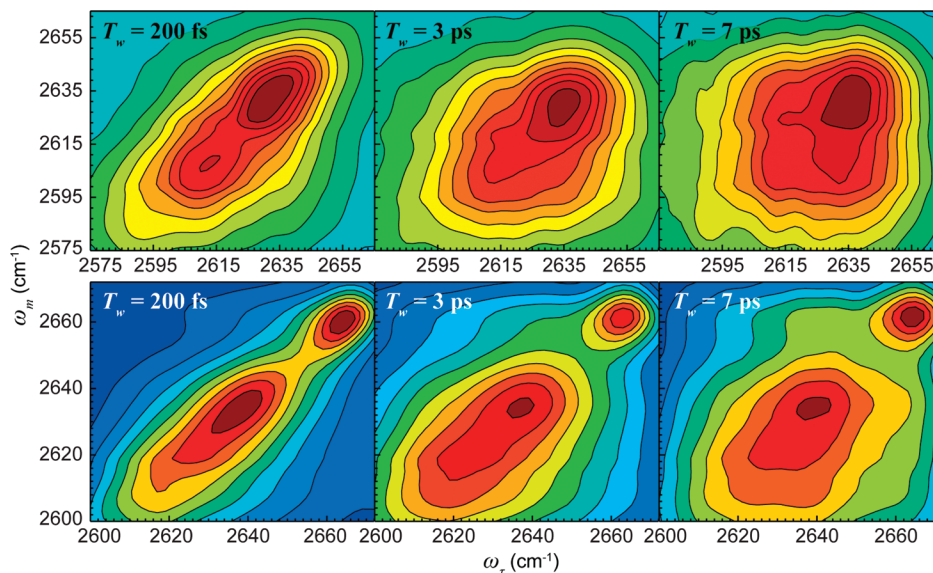


**Figure 3.** The  $0 \rightarrow 1$  transition region of the 2D IR chemical exchange spectra for deuterated phenol dissolved in phenylacetylene (top panel) and in the mixed solvent, phenylacetylene/carbon tetrachloride (bottom panel). Chemical exchange causes off-diagonal peaks to grow in as  $T_w$  increases.

tions of the exponentially time-dependent signals measured in ultrafast infrared pump–probe spectroscopy; however, instead of exponentials of scalars, the solution is the sum of two matrix exponentials.<sup>26</sup>

In past measurements of chemical exchange, the peaks in the 2D IR spectra have been fit to 2D Gaussians to extract the rates of chemical exchange.<sup>25,26</sup> This type of analysis requires that the peaks are relatively well separated. The highly overlapping peaks of the phenol in pure phenylacetylene or the phenol in phenylacetylene and carbon tetrachloride systems are not separated enough to apply the Gaussian fitting method. Therefore, to analyze the data in the current study, a somewhat different approach is taken which is capable of determining the time dependence of R and T state chemical exchange. This approach involves analyzing the time-dependent relative amplitudes of the peak in a series of 2D IR spectra. Each experimental peak amplitude is modeled as the sum of the contributions of overlapping Gaussians. Each Gaussian corresponds to a specific exchanging subensemble and is also weighted by its dependence on the species transition dipoles. The simulated and experimental peak amplitudes are compared in order to find the best input parameters that describe the experimental data.

From the absorption spectrum of phenol dissolved in pure phenylacetylene (Figure 2a), we know that the peaks of the R and T states are at frequencies  $\omega_R$  and  $\omega_T$ , respectively. In the 2D spectra, a point is located at  $(\omega_r, \omega_m)$ . Then the two diagonal peaks are located at  $(\omega_r, \omega_r)$  and  $(\omega_t, \omega_t)$ . The  $R \rightarrow T$  off-diagonal peak will occur at  $(\omega_r, \omega_t)$  and the  $T \rightarrow R$  off-diagonal peak will occur at  $(\omega_t, \omega_r)$ . Therefore, within the experimental uncertainties of the frequencies  $\omega_R$  and  $\omega_T$ , the peak locations of the two diagonal and two off-diagonal bands are known. Because the four 2D bands overlap, the signal at the known position for each peak has a contribution from overlap with the other peaks that is accounted for.

The transition dipoles are not the same for the R and T absorptions. The observed amplitudes of the diagonal R and T peaks depend on their populations scaled by  $(\mu_R)^4$  and  $(\mu_T)^4$ , respectively. The off-diagonal peaks are scaled by  $(\mu_R)^2(\mu_T)^2$ . The equilibrium constant determined from the 2D IR experiments was compared with that measured from the linear IR

absorbance spectrum to ensure agreement between linear and 2D spectroscopic data sets. For an appropriate choice of transition dipole ratios, the linear and 2D spectroscopic data will be consistent. This approach is similar to other methods used for determining transition dipole ratios for vibrational oscillators.<sup>32</sup> The transition dipole ratio,  $(\mu_T/\mu_R)$ , was determined to be 1.16. The equilibrium constant ( $K_{\text{eq}} = [T]/[R]$ ) for the exchange reaction was found from the 2D IR to be 0.74 and from the linear IR spectrum to be 0.83, which is quite reasonable agreement. The various parameters were varied somewhat in the final fitting process (see below).

The time-dependent populations are simulated by the kinetic model discussed above. Given the linear IR spectrum, the measured transition dipole ratio for the R and T bands, the measured vibrational lifetimes and rotational diffusion constants, the 2D IR spectrum can be generated. The line widths from linear IR are used to generate the overlap factors using a two-dimensional Gaussian line shape. The input lifetimes and orientational diffusion constant ( $D_R$ ) data are generated by iteratively fitting polarization-selective pump–probe data and 2D IR relative amplitude data including the effects of exchange.<sup>30</sup> The orientational relaxation time constants ( $1/6D_R$ ) of the two states were assumed to be the same (5.6 ps), which is reasonable considering the small differences in shape and volume of the R and T states. The OD stretch lifetimes were measured by iterative fitting of polarization-selective pump–probe data, which gave 6 ps for the R state and 8.7 ps for the T state. The  $R \rightarrow T$  and  $T \rightarrow R$  rate constants were adjusted until the model best fit the relative amplitude data measured from the experimental 2D IR spectrum. The method used to fit the data neglects spectral diffusion. However, since the line shapes have a large homogeneous component and spectral diffusion is relatively fast, the effect of neglecting spectral diffusion is minor.

The relative amplitude data from the 2D IR spectra and corresponding fits for deuterated phenol in pure phenylacetylene are shown in Figure 4. At each  $T_w$ , the amplitudes of the other three peaks are given relative to the R peak. The black symbols and line are the experimental data and fit for the diagonal T state. The red and green symbols and red line are the experimental data and fit for the two off-diagonal peaks,  $R \rightarrow T$  and  $T \rightarrow R$ . Because of the substantial overlap of the peaks,

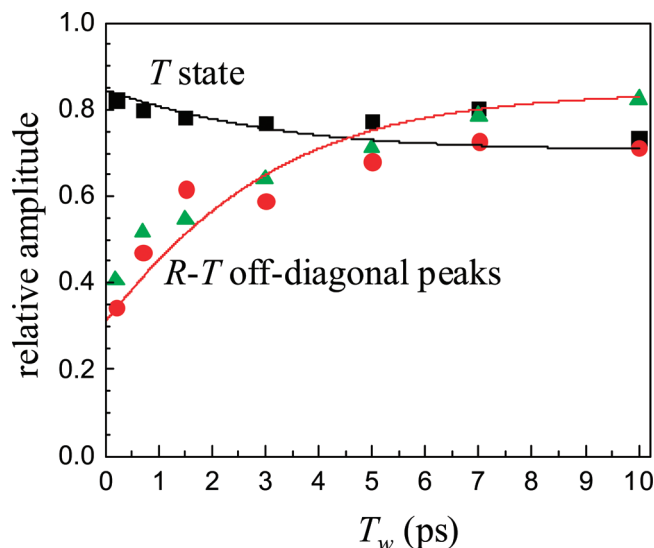


**Figure 4.** Relative peak amplitudes (squares, circles, triangles) for the phenol dissolved in phenylacetylene. All of the points are normalized by the R state amplitude. The black line is the fit T state amplitude. The red circles are the T  $\rightarrow$  R exchange off-diagonal peak amplitudes, and the green triangles are the R  $\rightarrow$  T exchange off-diagonal peak amplitudes. The red line is the fit for the off-diagonal peak amplitudes. The fits yield the T  $\rightarrow$  R exchange time constant of 4.2 ps (see text).

there is significant scatter in the data. Nonetheless, clear growth is shown for the off-diagonal peaks, which is evident qualitatively from the top panels of Figure 3. The fit results in a T  $\rightarrow$  R time constant of 4.2 ps. Consistent fits resulting in exchange times between 3 and 6 ps could also be achieved by varying input parameters, such as the equilibrium constant or the transition dipole ratio. The times, 3 and 6 ps, are the extremes that did not produce impossible contradictions with any of the types of data. Thus, it takes  $\sim 4.5$  ps for a deuterated phenol bound to the triple bond of phenylacetylene to migrate to the hydrogen-bond-accepting site on the phenyl ring. For the T  $\rightarrow$  R time constant,  $\tau_{TR} = 4.5$  ps and the equilibrium constant of  $\sim 0.8$ , then the R  $\rightarrow$  T time constant,  $\tau_{RT} = 5.6$  ps. Given the error range for the fits and error bars for some of the input parameters, it is not clear that the difference in the two time constants is significant. Nonetheless, the results clearly demonstrate the chemical exchange between the T and R states with a time constant of about 4–5 ps.

**C. Determining the Exchange Mechanism.** Despite measuring that the time for exchange between the T and R states is about 4.5 ps, we have not yet identified the *mechanism* of exchange. As discussed in the Introduction, the exchange process could proceed through direct migration along the molecule or via two other possible mechanisms. The other mechanisms are intermolecular hopping, i.e., a phenol goes directly from the T state on one molecule to the R state on a different molecule and vice versa, or migration through a “free,” non-hydrogen-bonding state. These other mechanisms can be tested by diluting the phenylacetylene solvent with carbon tetrachloride.

When phenylacetylene is diluted, the non-hydrogen-bonding (free) state of phenol, which may exist at very low concentration in the pure phenylacetylene sample, achieves a significant concentration relative to the hydrogen-bonded states of phenol. The absorption spectrum is shown in Figure 2B, in which the free state peak is prominent. The time-dependent 2D IR spectra in the mixed solvent yield all six rate constants for the exchange processes between the three spectroscopic states. For a system

that undergoes exchange through the free state, the off-diagonal peaks between the free peak (F) and the T and R peaks will grow in first and the TR off-diagonal peak will grow in subsequently.

The mixed solvent experiment also allows us to examine whether the exchange process occurs via direct hydrogen bond migration or by intermolecular hopping exchange. Any intermolecular exchange process will show different pseudo-first-order kinetics depending on the equilibrium concentration of the exchange reagents. The hydrogen bond exchange reaction here will then be formally second order. By decreasing the amount of phenylacetylene in the system, the available phenylacetylene hydrogen-bonding sites in the first solvation shell will decrease. For a system that only undergoes intermolecular hopping, a linear decrease in the rate constant proportional to the concentration of phenylacetylene would be anticipated. Therefore, by diluting the phenylacetylene solvent with carbon tetrachloride and comparing the exchange time between the T and R states, we can distinguish between direct hydrogen bond migration and intermolecular hopping.

The three bottom panels of Figure 3 display representative 2D IR correlation spectra for deuterated phenol dissolved in phenylacetylene/ $\text{CCl}_4$ . In this solution, the volume fraction (mol/L) of phenylacetylene is reduced by a factor of 2.5. Again, only the 0  $\rightarrow$  1 portions of the spectra are shown. The diagonal peak for the free state is clearly visible and occurs at the 2D frequencies predicted from the linear IR spectrum. There is clear growth of all six off-diagonal peaks in these spectra. Figure 5 displays the experimental results and the fits (discussed below) of the 2D IR spectroscopic data. The top panel shows the R and T state amplitudes divided by the amplitude of the free state. From top to bottom, the remaining panels show the T–R, R–F, and T–F off-diagonal relative peak amplitudes. There is growth of all six off-diagonal peaks as  $T_w$  increases. From the data alone, it is clear that the T–R off-diagonal peaks grow much faster than the R–F and T–F off-diagonal peaks. The R–T peaks rise rapidly and have essentially reached a plateau by  $\sim 5$  ps. In contrast the R–F and T–F peaks rise much more gradually and are still increasing at 20 ps. The rapid increase in the R–T peaks compared to the R–F and T–F peaks rules out the mechanism in which the free state is an intermediate in the RT exchange. If the free state is an intermediate, the R–F and T–F peaks must grow prior to the R–T peaks.

The data analysis procedures discussed above were also used for the three-state system, and the results are shown in Figure 5. Parameters for the overlap and peak position were obtained from the linear absorbance spectra. The spectroscopic parameters are given in connection with Figure 2. The transition dipole ratio T/R was set to 1.16 as above. The ratio for R/F was set to 1.30. This ratio was determined previously.<sup>8,26</sup> The OD stretch vibrational lifetimes for the hydrogen-bonded states were taken to be the same as those used for the pure phenylacetylene system, and the vibrational lifetime for the free state was taken to be 11.8 ps, as previously measured.<sup>36</sup> The orientational relaxation times ( $1/6D_R$ ) for the hydrogen-bonding states were corrected for the increase in solvent viscosity using the Debye–Stokes–Einstein equation.<sup>25</sup> The phenylacetylene/carbon tetrachloride mixture has a viscosity 3.5% higher than pure phenylacetylene, resulting in orientational relaxation times of 5.8 ps. The orientational relaxation time for the free state was measured previously to be 2.5 ps in pure  $\text{CCl}_4$ . This value was used because the viscosity of the mixed solvent is only 1% higher than that for  $\text{CCl}_4$ . The equilibrium concentration ratio of the T state to the F state ( $[T]/[F]$ ) was found to be 1.1

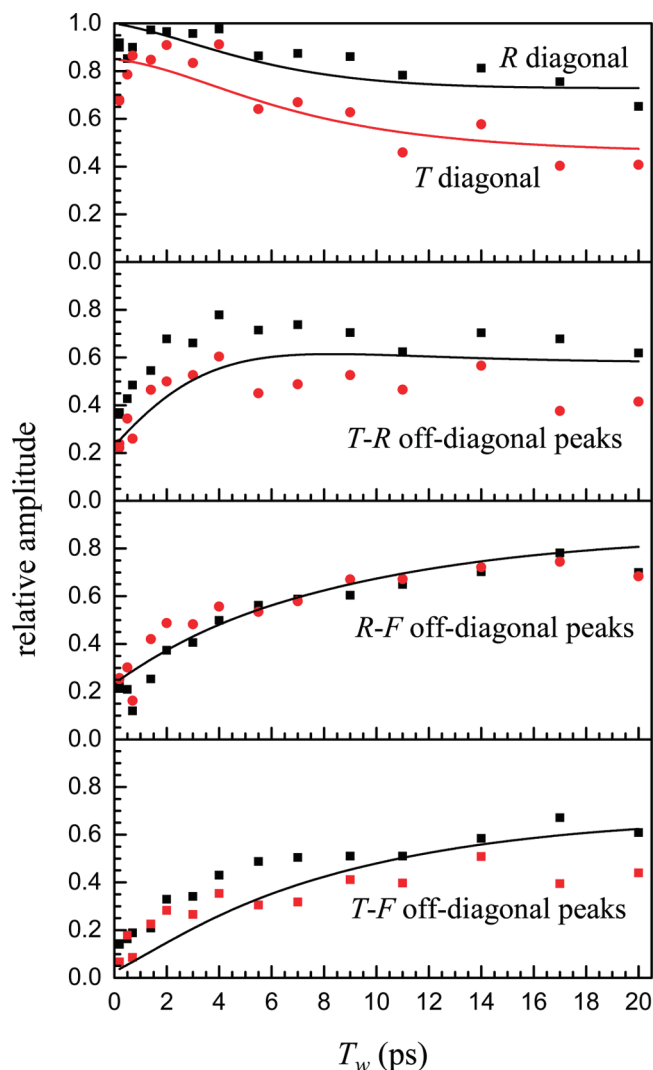


**Figure 5.** Panels from top to bottom: the amplitudes of the R and T diagonal peaks, the T–R, the R–F, and the R–T off-diagonal peaks all normalized to the diagonal F peak. The curves are the simultaneous fits to all of the data. In the off-diagonal peak plots, the black squares are the T → R, R → F, and T → F data, and the red circles are the reverse process data. See text for discussion of trends.

from the 2D IR data and 1.0 from the linear IR data, which agree well given the experimental uncertainties and the number of parameters involved. The equilibrium concentration ratio of the R and F states ( $[R]/[F]$ ) was found to be 1.8 from the 2D IR data and 1.4 from the linear absorbance data. This disagreement resulted from difficulty in replicating the early time amplitude data for the R state diagonal peak in the 2D spectra. Systematic variation of the transition dipole ratios results in better agreement between the equilibrium constants determined from the two types of spectra but worse fitting of the early time 2D IR data. The difference in the two values did not result in a significant change in the R ↔ T time constant given below. Examining Figure 5, it is clear that portions of the experimental data are not fit well by the simulated curves. Overemphasis on fitting the early time data, for example on the T–F peak, can result in nonphysical (negative) results for the time constants. We therefore found the most consistent physical model for the data. The ranges for exchange times reported below reflect all models that were physical and reproduce the data to a similar degree.

Using these input parameters, the data were fit (solid curves in Figure 5). The time constant for the T → R exchange is 5.3

ps, for R → F is 16 ps, and for T → F is 45 ps. As discussed qualitatively above, the T–R exchange is much faster than the T–F and for R–F exchange processes. These exchange times rule out the mechanism in which the T–R exchange occurs with the free state as an intermediate.

The intermolecular hopping mechanism is formally second order and, therefore, should slow down linearly as the concentration of available phenylacetylene molecules is lowered. The intramolecular migration mechanism rate should remain constant despite dilution due to the constant 1:1 ratio between the two phenylacetylene hydrogen bond accepting sites. The important number from the above analysis is that the T → R exchange time is 5.3 ps in the mixed solvent phenylacetylene/ $\text{CCl}_4$ . This value should be compared to the T → R exchange time of 4.2 ps in pure phenylacetylene. Considering reasonable variations in the other parameters, the mixed solvent exchange time falls within the 3–6 ps range of fitting results. The result is that either the exchange time did not change within experimental error when the phenylacetylene was diluted or there is a small increase in time. The concentration of phenylacetylene in the pure phenylacetylene sample was 9.1 M, while the concentration in the sample diluted with carbon tetrachloride was 3.7 M. If the exchange event occurred via intermolecular hopping, then the increase in exchange time would scale inversely with the concentration of phenylacetylene. The dilution would result in an increase by a factor of 2.5. The result would be an exchange time of 10.5 ps if intermolecular hopping was the dominant mechanism. Ten picoseconds is well outside the largest possible error in the measured exchange times, leading to the conclusion that the exchange between the two states occurs via intramolecular hydrogen bond migration event. If the difference between the exchanges times in the pure solvent (4.2 ps) and the mixed solvent (5.3 ps) is real, it is not unreasonable. In going to the mixed solvent, the viscosity increased and solvation structure around the phenol/phenylacetylene complex is substantially different. These factors can lead to the somewhat different exchange times.

The argument for the direct exchange mechanism is bolstered further when the intermolecular hopping mechanism is considered in a little more detail. If the phenol hops from one phenylacetylene to another, there are four types of hops, T → R, R → T, T → T, and R → R. The last two are not observed in the 2D IR measurement since the OD stretch will start and end in the same peaks. These last two types of hops do not contribute to the growth of off-diagonal peaks. Approximately half of the hops for intermolecular exchange would not contribute to the measured growth of the off-diagonal peaks. Therefore, the actual intermolecular jump time of the phenol between phenylacetylene molecules would be ~2.5 ps given the measured growth of the off-diagonal peaks of 4–5 ps. This time is not consistent with other measurements made on  $\pi$ -hydrogen-bonding systems where the fastest time observed is 6 ps for the dissociation of the very weakly bound phenol/bromobenzene complex to go to the phenol-free state.<sup>5,26</sup> The net result is that all of the evidence supports the intramolecular direct hydrogen bond migration from one hydrogen bonding site to another.

#### IV. Concluding Remarks

The direct migration of a  $\pi$ -hydrogen-bonded phenol molecule between sites of the conjugated  $\pi$  electron system of phenylacetylene has been observed using 2D IR chemical exchange spectroscopy. The time scale of this migration was measured to be ~5 ps. Both exchange via a free state

intermediate mechanism and an intermolecular hopping mechanism were ruled out as viable alternatives by performing 2D IR spectroscopy on phenol dissolved in a phenylacetylene/carbon tetrachloride mixed solvent. We emphasize that despite the significant error bars on the hydrogen bond migration time, the migration mechanism is the only mechanism consistent with the data. Both of the alternative mechanisms have been ruled out. The identification of the exchange mechanism as direct hydrogen bond migration between sites on a single molecule is the most significant result of the experiments.

An important implication of the observation of direct migration is the ability of electrophiles to move continuously across a conjugated aromatic surface. The electrostatic interactions between electrophiles and conjugated aromatic systems occur whenever a large conjugated polymer folds into a nonextended structure or when solvents interact directly with conjugated aromatic systems. Our measurements suggest that electrophiles against the aromatic surface maintain mobility and can move across heterogeneities in the  $\pi$  electron density.

**Acknowledgment.** This research was supported by a grant from the Air Force Office of Scientific Research (F49620-01-1-0018), the National Institutes of Health (2-R01-GM061137-09), and the National Science Foundation (DMR 0652232). D.E.R. thanks the Fannie and John Hertz Foundation, the Stanford Graduate Fellowship program, and the National Science Foundation Graduate Research Fellowship Program for fellowships.

## References and Notes

- (1) Steiner, T.; Koellner, G. *J. Mol. Biol.* **2001**, *305*, 535.
- (2) Meyer, E. A.; Castellano, R. K.; Diederich, F. *Angew. Chem., Int. Ed.* **2003**, *42*, 1210.
- (3) Hagan, M. F.; Chandler, D. *Biophys. J.* **2006**, *91*, 42.
- (4) Huggins, C. M.; Pimentel, G. C. *J. Phys. Chem.* **1956**, *60*, 1615.
- (5) Zheng, J. R.; Fayer, M. D. *J. Am. Chem. Soc.* **2007**, *129*, 4328.
- (6) Kwak, K.; Lee, C.; Jung, Y.; Han, J.; Kwak, K.; Zheng, J. R.; Fayer, M. D.; Cho, M. *J. Chem. Phys.* **2006**, 125.
- (7) Yoshida, Z.; Ozoe, H.; Ishibe, N. *J. Am. Chem. Soc.* **1972**, *94*, 4948.
- (8) Tsubomura, H. *J. Chem. Phys.* **1956**, *24*, 927.
- (9) Sedlak, R.; Hobza, P.; Patwari, G. N. *J. Phys. Chem. A* **2009**, *113*, 6620.
- (10) Singh, P. C.; Bandyopadhyay, B.; Patwari, G. N. *J. Phys. Chem. A* **2008**, *112*, 3360.
- (11) Singh, P. C.; Patwari, G. N. *J. Phys. Chem. A* **2008**, *112*, 4426.
- (12) Singh, P. C.; Patwari, G. N. *J. Phys. Chem. A* **2008**, *112*, 5121.
- (13) Hasegawa, K.; Masuda, T.; Higashimura, T. *Macromolecules* **1975**, *8*, 255.
- (14) Sapse, A. M.; Jain, D. C. *Int. J. Quantum Chem.* **1988**, *33*, 69.
- (15) Hunter, C. A.; Sanders, J. K. M. *J. Am. Chem. Soc.* **1990**, *112*, 5525.
- (16) Hunter, C. A. *Angew. Chem., Int. Ed.* **2004**, *43*, 5310.
- (17) Elmer, S. P.; Pande, V. S. *J. Chem. Phys.* **2005**, 122.
- (18) Ray, C. R.; Moore, J. S. *Supramolecular Organization of Foldable Phenylene Ethynylene Oligomers*. In *Poly(Arylene Ethynylene)s: From Synthesis to Application*; Springer-Verlag: Berlin, 2005; Vol. 177, p 91.
- (19) Zang, L.; Che, Y. K.; Moore, J. S. *Acc. Chem. Res.* **2008**, *41*, 1596.
- (20) Zhang, W.; Moore, J. S. *Angew. Chem., Int. Ed.* **2006**, *45*, 4416.
- (21) Lam, J. W. Y.; Tang, B. Z. *Acc. Chem. Res.* **2005**, *38*, 745.
- (22) Sinnokrot, M. O.; Sherrill, C. D. *J. Am. Chem. Soc.* **2004**, *126*, 7690.
- (23) Xie, Z. Q.; Liu, L. L.; Yang, B.; Yang, G. D.; Ye, L.; Li, M.; Ma, Y. G. *Cryst. Growth Des.* **2005**, *5*, 1959.
- (24) Kim, Y. S.; Hochstrasser, R. M. *Proc. Natl. Acad. Sci.* **2005**, *102*, 11185.
- (25) Zheng, J. R.; Kwak, K.; Asbury, J.; Chen, X.; Piletic, I. R.; Fayer, M. D. *Science* **2005**, *309*, 1338.
- (26) Kwak, K.; Zheng, J. R.; Cang, H.; Fayer, M. D. *J. Phys. Chem. B* **2006**, *110*, 19998.
- (27) Zheng, J. R.; Kwak, K. W.; Xie, J.; Fayer, M. D. *Science* **2006**, *313*, 1951.
- (28) Ishikawa, H.; Kwak, K.; Chung, J. K.; Kim, S.; Fayer, M. D. *Proc. Natl. Acad. Sci. U.S.A.* **2008**, 105.
- (29) Kwak, K.; Rosenfeld, D. E.; Chung, J. K.; Fayer, M. D. *J. Phys. Chem. B* **2008**, *112*, 13906.
- (30) Moilanen, D. E.; Wong, D.; Rosenfeld, D. E.; Fenn, E. E.; Fayer, M. D. *Proc. Natl. Acad. Sci. U.S.A.* **2009**, *106*, 375.
- (31) Fayer, M. D.; Moilanen, D. E.; Wong, D.; Rosenfeld, D. E.; Fenn, E. E.; Park, S. *Acc. Chem. Res.* **2009**, *42*, 1210.
- (32) Zheng, J. R.; Kwak, K.; Chen, X.; Asbury, J. B.; Fayer, M. D. *J. Am. Chem. Soc.* **2006**, *128*, 2977.
- (33) Kwak, K. W.; Park, S.; Fayer, M. D. *Proc. Natl. Acad. Sci. U.S.A.* **2007**, *104*, 14221.
- (34) Asbury, J. B.; Steinel, T.; Stromberg, C.; Gaffney, K. J.; Piletic, I. R.; Goun, A.; Fayer, M. D. *Chem. Phys. Lett.* **2003**, *374*, 362.
- (35) Park, S.; Kwak, K.; Fayer, M. D. *Laser Phys. Lett.* **2007**, *4*, 704.
- (36) Rosenfeld, D. E.; Gengeliczki, Z.; Fayer, M. D. *J. Phys. Chem. B* **2009**, *113*, 13300.
- (37) Maity, S.; Patwari, G. N. *J. Phys. Chem. A* **2009**, *113*, 1760.

JP911452Z